Direct Observation of Nanocrystallite Buckling in Carbon Fibers under Bending Load

D. Loidl,[1] O. Paris,[2] M. Burghammer,[3] C. Riekel,[3] and H. Peterlik[1,*]

[1]*Institute of Materials Physics, University of Vienna, Boltzmanngasse 5, A-1090 Vienna, Austria*
[2]*Department of Biomaterials, Max-Planck-Institute of Colloids and Interfaces, 14424 Potsdam, Germany*
[3]*European Synchrotron Radiation Facility, 6 Rue Jules Horowitz, B.P. 220, F-38043 Grenoble Cedex 9, France*

(Received 5 April 2005; published 21 November 2005)

Single carbon fibers are deformed in bending by forming loops with varying radius. Position-resolved x-ray diffraction patterns from the bent fibers are collected from the tension to the compression region with a synchrotron radiation nanobeam of 100 nm size from a waveguide structure. A strain redistribution with a shift of the neutral axis is observed. A significant increase of the misorientation of the graphene sheets in the compression region shows that intense buckling of the nanosized carbon crystallites is the physical origin of different tensile and compressive properties.

DOI: 10.1103/PhysRevLett.95.225501 PACS numbers: 61.66.Bi, 61.10.Eq, 62.20.Dc, 62.25.+g

Oriented, fibrous materials such as carbon fibers [1] or carbon nanotubes [2] are governed to a major extent by the extreme anisotropy between the in-plane (covalent) and out-of-plane (van der Waals) bonding forces, which is the source of many particularities in their mechanical properties. The basic structural units, or crystallites, of high performance carbon fibers are planar structures, with a lateral extension L_a of typically some nanometers and a stacking height L_c in the same order of magnitude [3], whereas they are tubelike for single-wall or multiwall carbon nanotubes (CNT). Both planar and tubelike structures provide extraordinary mechanical properties in tension, such as a Young's modulus above 1 TPa [4–6]. Therefore, carbon fibers themselves can be seen as a model system to study the mechanical properties of carbon based nanocomposite materials. Axial compressive strength often limits the use of composite materials as a consequence of Euler buckling [7]. For CNT, this was previously investigated by atomic force microscopy [8], whereas data on the compressive properties of composites based on CNT are rare [9]. Though the weak bonding of CNT within a CNT bundle can be improved by cross-linking them with electron irradiation [10], widely used technical applications with CNT as reinforcing elements are still missing. The situation is completely different for planar carbon nanostructures such as carbon fibers, where a huge amount of scientific literature as well as numerous technical implementations exist [11].

The compressive strength of carbon fibers (diameter of 5–10 μm) can be determined by the loop test, the bending beam, the single-fiber composite, the recoil, and the single-fiber compression test (see [12] for an overview). For the compressive Young's modulus, only a few approaches were reported due to the difficulty in achieving a sufficient strain resolution, e.g., using the onset of Euler buckling of short fiber pieces [13] or the correlation of the D-band shift in Raman spectroscopy to the fiber strain [14].

Related microstructural investigations to study the mechanisms of compressive deformation in carbon fibers are also quite limited and exclusively based on *ex situ* studies after deformation or fracture of the specimens, e.g., by TEM [15], scanning electron microscopy [7,16], and x-ray diffraction [17]. Different failure mechanisms were proposed for low and high modulus fibers, such as buckling on the compression side or shear kink bands developing across the entire fiber, respectively [16]. Whereas probing structural changes by *in situ* microbeam x-ray diffraction using synchrotron radiation during tensile loading is quite established [4,18], no direct measurement of the development of the structure at the nanometer scale during compressive loading has, to our knowledge, been performed. In the present Letter, we report the observation of nanostructural changes during bending deformation of single carbon fibers. We realized a loading situation in bending by forming carbon fiber loops and combined it with position-resolved scanning x-ray diffraction enabled by a waveguide structure coupled to a synchrotron radiation undulator source [19,20]. By precisely aligning the elongated x-ray source of 100 nm $\times$ 3 μm with the axis of the fiber, successive diffraction patterns of bent fibers could be collected with a resolution of 100 nm while scanning the fiber across the beam from the tension to the compression region.

For the experiments, we used carbon fibers from the main precursor routes [11,21] based on polyacrylonitrile (PAN fibers) or mesophase pitch (MPP fibers). The MPP fibers were chosen to cover a wide range of Young's moduli and associated structural parameters; the PAN fibers (HTA5131) were heat treated at 1800, 2100, and 2400 °C to obtain the same effect (denoted by HT00 for the as-received fiber and HT18, HT21, and HT24 for the respective heat treatment). Detailed fiber properties were described in a previous paper [4].

The experimental setup is depicted in Fig. 1: A carbon fiber loop is formed by threading the ends of the fiber through a hollow needle, where the bending radius R_b determined in an on-line light microscope is simply varied by pulling down the ends of the fiber. The experiment was

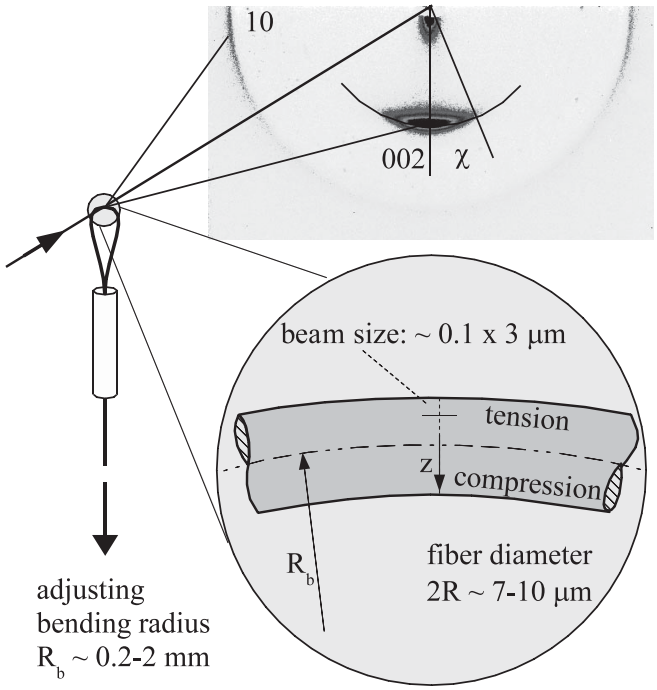

FIG. 1. Sketch of the experimental setup for scanning single bent fibers. The distance between the waveguide exit and the fiber was less than 10 microns.

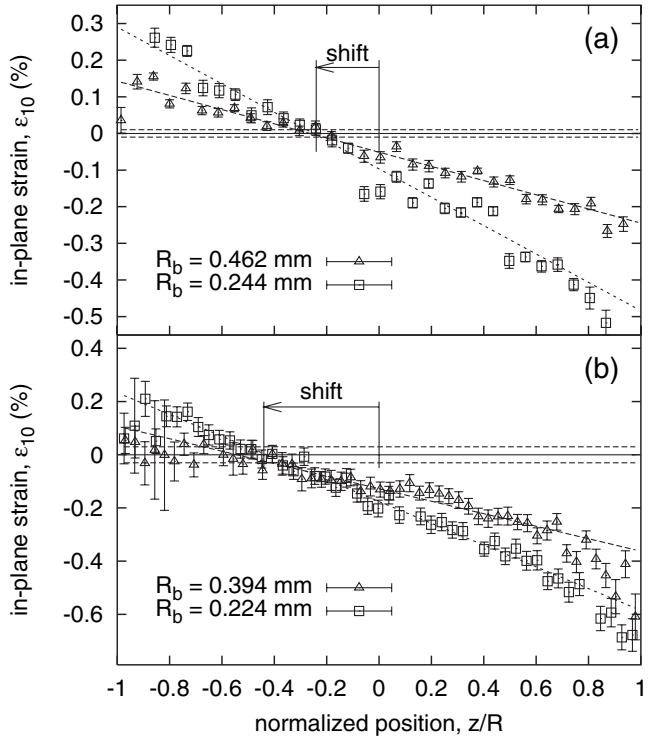

FIG. 2. In-plane strain distribution across (a) the PAN fiber HT21 and (b) the MPP fiber E35 for two different bending radii. The values for the unbent fibers with standard errors are inserted as solid and dashed lines, respectively. The shift of the neutral axis is indicated by the arrows.

performed at the microfocus beam line (ID13) of the European Synchrotron Radiation Facility with the scanning setup [22], a wavelength of 0.976 Å, and an area detector (MarCCD). Each bent fiber was scanned with 200 nm steps from the tension to the compression region. Corresponding scanning of unbent fibers gave the unstrained reference values. Two main parameters were evaluated from the 2D diffraction patterns (see Fig. 1): The position of the 10 reflection gives the in-plane distance d_{10} of the carbon atoms in loading direction, and the microstrain of the fiber is obtained by $\varepsilon_{10}(z) = [d_{10}(z) - d_{10}(0)]/d_{10}(0)$, the parameter z being the position within the fiber and 0 denoting the reference value, obtained from the average value of the scan across the unstrained fiber. The second parameter is the azimuthal width (half width at half maximum) χ_{002} of the 002 reflection, describing the deviation of the orientation of the graphene planes with respect to the fiber axis. Figure 2 shows the in-plane strain within the graphene sheets, $\varepsilon_{10}(z)$, exemplarily for the PAN fiber HT21 and the MPP fiber E35 for two different bending radii. The in-plane strain varies roughly linear with position; however, the neutral zone is not located in the center of the fiber but is shifted towards the tension region. This shift is nearly independent of the bending radius but differs between the individual fibers and is much larger for E35 [Fig. 2(b)] in comparison to HT21 [Fig. 2(a)]. Generally, a considerably higher shift was observed for all MPP fibers in comparison to PAN fibers.

The azimuthal width χ_{002} of the unbent PAN fiber HT21 [Fig. 3(a)] shows a constant value except a remarkable decrease at the fiber boundaries, which is related to a skin-core morphology. A higher orientation of the skin of PAN fibers was previously deduced from TEM images [23] and microbeam diffraction [24]. The bent fiber shows a linear increase of χ_{002} from the tension into the compression region apart from the fiber boundary, indicating an increase of the fiber orientation upon tension and a corresponding decrease upon compression, with a similar shift of the neutral zone as observed for the strain in Fig. 2(a). Different to the nearly linear increase of χ_{002} within the fiber core of the PAN fibers [Fig. 3(a)], χ_{002} of the MPP fiber E35 tends to a constant value towards the fiber boundary in the tension region, but in the compression region an enormous increase of the azimuthal width up to almost a factor 2 is observed [Fig. 3(b)]. This is clear evidence for extensive buckling on the nanoscale and was found for all MPP fibers to a similar amount. Buckling can happen on the scale of single crystallites with a stacking height of 2–10 nm (depending on the respective type of fiber) or on the level of single graphene sheets with an interplanar distance of approximately 0.34 nm. There are two clear indications that buckling takes place on the crystallite level: (i) The layer distance d_{002} of the lattice planes is nearly unchanged

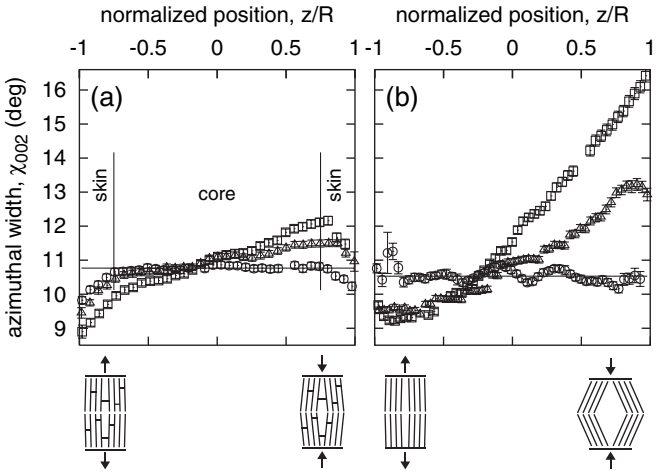

FIG. 3. Azimuthal width of graphene planes χ_{002} across (a) the PAN fiber HT21 and (b) the MPP fiber E35 for the unbent fiber (open circles) and for two different bending radii (symbols are the same as in Fig. 2). The solid line is the mean value of the unbent fiber (for HT21 taken only from the core region). The scheme visualizes the different compression behavior of PAN and MPP fibers.

during loading (changes less than 0.1%), and (ii) the stacking height of the crystallites, L_c, does not show any differences between the tension and the compression part of the bent fiber.

The apparent shift of the neutral axis was, to the best of our knowledge, never considered in the literature on testing compressive properties of carbon fibers. From the shift of the neutral axis, integration over the respective areas directly gives the Young's moduli in tension and compression (E_t and E_c), if regions with constant elastic properties are assumed [25]:

$$E_t \int_1 dAz + E_c \int_2 dAz = 0, \tag{1}$$

the labels 1 and 2 denoting the integration range over the tension and compression area, respectively. Equation (1) can be analytically solved for a circular cross section:

$$\frac{E_c}{E_t} = \frac{4\sqrt{1-a^2} + 2a^2\sqrt{1-a^2} + 3a\pi + 6a\,\mathrm{arcsin}a}{4\sqrt{1-a^2} + 2a^2\sqrt{1-a^2} - 3a\pi + 6a\,\mathrm{arcsin}a}, \tag{2}$$

with $a = z_s/R$ being the ratio of the shift of the neutral zone z_s to the fiber radius R. The sign convention is chosen that a is negative (located in the tension region) as depicted in Fig. 2. The larger the shift of the neutral zone, the higher the ratio of the Young's modulus in tension to the one in compression. The maximum stress occurs at the fiber boundary [25]

$$\frac{\sigma_t}{\sigma_c} = \frac{z_t E_t}{z_c E_c}, \tag{3}$$

with z_t and z_c denoting the distances from the neutral axis to the respective boundary of the fiber. An additional strain dependence of both the compression and the tensile modulus is probable, because nonlinearity was frequently reported for carbon fibers in tension [26] as well as in compression [27]. As the results for different bending radii and, thus, different strains showed no pronounced difference in the position of the neutral axis (see Fig. 2), we suggest that this effect is small in comparison to the differences from varying processing parameters.

In Table I, all results are listed for the different types of fibers. The position of the neutral axis was derived by a linear fit of the strain data (see Fig. 2), and the ratio of the compressive and tensile Young's moduli and stresses (E_c/E_t, E_c and σ_c/σ_t, respectively) were evaluated from Eqs. (2) and (3). The error was obtained from the uncertainty of the shift of the neutral axis with respect to the standard error of the unbent reference fiber. The Young's modulus in tension E_t was obtained from single-fiber tensile tests, and the in-plane coherence length L_a and the stacking height L_c of the crystallites were derived by applying the Scherrer equation to the 10 and 002 reflections, respectively [28]. It is obvious from Table I that the PAN fibers exhibit superior compressive properties in comparison to MPP fibers even for comparable lateral crystallite size L_a. L_a is not the decisive parameter, which would be the case for buckling from gliding of single adjacent planes. PAN and MPP fibers exhibit a different deformation behavior, i.e., PAN fibers a continuous deformation with modulus softening in compression and hardening in tension as suggested by the continuous D-band shift in Raman spectroscopy [14] and MPP fibers buckling in the compression range. This difference is attributed to the existence of covalent cross-links connecting the crystallites and their graphene layers. These cross-links were modeled by first-principles calculations [29] and experimentally reported for CNT in bundles induced by high-energy particle radiation [10]. An experimental verification for carbon fibers is difficult as only few cross-links are expected. The existence of cross-links may be deduced from the higher shear modulus of PAN fibers in comparison to MPP fibers, obtained from the smaller decrease of χ_{002} in single-fiber tension tests [4]. Further evidence for the existence of cross-links is provided by the lower electrical conductivity of PAN fibers compared to MPP fibers with similar in-plane coherence lengths (derived from x-ray scattering) and phonon mean free path for boundary scattering (from modeling thermal conductivity measurements) [30,31]. Such cross-links could be formed during processing of PAN fibers, as incomplete ladder polymer structures are formed with high defect concentrations easing the formation of cross-links. The situation is different for MPP fibers, where the mesophase-pitch precursor provides perfect liquid crystalline structures being assembled during the spinning process. No cross-linking and, consequently, very limited resistance against buckling on the

TABLE I. Summary of results for the investigated fibers. The low Young's modulus for the MPP fibers is the postbuckling modulus.

Fiber	Precursor	Producer	L_a (nm)	L_c (nm)	E_t (GPa)	E_c/E_t	E_c (GPa)	σ_c/σ_t
HT00	PAN	Tenax	2.5	1.5	214	0.72 ± 0.09	155 ± 18	0.89
HT18	PAN	Tenax	4.0	2.5	256	0.47 ± 0.06	121 ± 14	0.65
HT21	PAN	Tenax	5.2	3.8	320	0.31 ± 0.04	100 ± 12	0.51
HT24	PAN	Tenax	5.8	5.3	378	0.33 ± 0.04	123 ± 15	0.52
K321	MPP	Mitsubishi	3.3	1.6	140	0.12 ± 0.03	17 ± 5	0.29
E35	MPP	DuPont	5.5	3.6	203	0.10 ± 0.03	20 ± 6	0.31
F500	MPP	Tonen	8.0	9.8	373	0.074 ± 0.02	28 ± 9	0.22
K137	MPP	Mitsubishi	9.4	12.5	509	0.075 ± 0.02	38 ± 12	0.22

crystallite level may, therefore, be expected for MPP fibers, in accordance with our experimental results.

In conclusion, position-resolved *in situ* scanning diffraction of bent carbon fibers shows the formation of a strain redistribution within the fibers and the neutral axis shifts considerably with respect to the fiber center. The physical origin of this shift is the extensive buckling of nanocrystallites in the compression region of MPP fibers. The results of the present work are believed to be of considerable technological interest, because carbon fiber reinforced composites are frequently produced from 2D or 3D woven prepregs with an inevitable strong curvature of the fibers. It also enlights the problem, which has to be faced in composites made from CNT, as the alignment of the CNT is very challenging.

This support from the Austrian Science Funds, Project No. P16315, is gratefully acknowledged.

*Electronic address: herwig.peterlik@univie.ac.at

[1] W. Ruland, Adv. Mater. **2**, 528 (1990).
[2] S. Iijima, Nature (London) **354**, 56 (1991).
[3] M. Guigon, A. Oberlin, and G. Desarmot, Fibre Sci. Technol. **20**, 55 (1984).
[4] D. Loidl, H. Peterlik, M. Müller, C. Riekel, and O. Paris, Carbon **41**, 563 (2003).
[5] S. Akita, H. Nishijima, Y. Nakayama, F. Tokumasu, and F. Takeyasu, J. Phys. D **32**, 1044 (1999).
[6] M. M. J. Treacy, A. Krishnan, and P. N. Yianilos, Microsc. Microanal. **6**, 317 (2000).
[7] M. Shioya and M. Nakatani, Compos. Sci. Technol. **60**, 219 (2000).
[8] O. Lourie, D. M. Cox, and H. D. Wagner, Phys. Rev. Lett. **81**, 1638 (1998).
[9] E. Thostenson and T. Chou, Carbon **42**, 3015 (2004).
[10] A. Kis, G. Csanyi, J. Salvetat, T. Lee, E. Couteau, A. Kulik, W. Benoit, J. Brugger, and L. Forro, Nat. Mater. **3**, 153 (2004).
[11] E. Fitzer and L. M. Manocha, *Carbon Reinforcements and Carbon-Carbon Composites* (Springer, Berlin, 1998).
[12] N. Oya and D. J. Johnson, Carbon **37**, 1539 (1999).
[13] N. Oya and D. J. Johnson, Carbon **39**, 635 (2001).
[14] N. Melanitis, P. L. Tetlow, C. Galiotis, and S. B. Smith, J. Mater. Sci. **29**, 786 (1994).
[15] M. G. Dobb, H. Guo, D. J. Johnson, and C. R. Park, Carbon **33**, 1553 (1995).
[16] G. J. Hayes, D. D. Edie, and J. M. Kennedy, J. Mater. Sci. **28**, 3247 (1993).
[17] S. Kumar, D. P. Anderson, and A. S. Crasto, J. Mater. Sci. **28**, 423 (1993).
[18] J. Keckes, I. Burgert, K. Frühmann, M. Müller, K. Kölln, M. Hamilton, M. Burghammer, S. Roth, S. Stanzl-Tschegg, and P. Fratzl, Nat. Mater. **2**, 810 (2003).
[19] A. Cedola, S. Lagomarsino, S. D. Fonzo, W. Jark, C. Riekel, and P. Deschamps, J. Synchrotron Radiat. **5**, 17 (1998).
[20] F. Pfeiffer, C. David, M. Burghammer, C. Riekel, and T. Salditt, Science **297**, 230 (2002).
[21] D. D. Edie, Carbon **36**, 345 (1998).
[22] C. Riekel, Rep. Prog. Phys. **63**, 233 (2000).
[23] S. Bennett and D. Johnson, Carbon **17**, 25 (1979).
[24] O. Paris, D. Loidl, and H. Peterlik, Carbon **40**, 551 (2002).
[25] J. M. Gere and S. P. Timoshenko, *Mechanics of Materials* (Chapman and Hall, London, 1987).
[26] C. Reder, D. Loidl, S. Puchegger, D. Gitschthaler, H. Peterlik, K. Kromp, G. Khatibi, A. Betzwar-Kotas, P. Zimprich, and B. Weiss, Composites Part A **34**, 1029 (2003).
[27] H. M. Hawthorne, J. Mater. Sci. **28**, 2531 (1993).
[28] M. Endo, C. Kim, T. Karaki, T. Kasai, M. J. Matthews, S. D. M. Brown, M. S. Dresselhaus, T. Tamaki, and Y. Nishimura, Carbon **36**, 1633 (1998).
[29] R. H. Telling, C. P. Ewels, A. A. El-Barbary, and M. I. Heggie, Nat. Mater. **2**, 333 (2003).
[30] B. Nysten, J. P. Issi, R. Barton, Jr., D. R. Boyington, and J. G. Lavin, Phys. Rev. B **44**, 2142 (1991).
[31] N. C. Gallego and D. D. Edie, Composites Part A **32**, 1031 (2001).